Available online at www.sciencedirect.com
ScienceDirect
International Journal of Multiphase Flow 34 (2008) 602–613
International Journal of Multiphase Flow
www.elsevier.com/locate/ijmulflow

Elongated bubbles in microchannels. Part II: Experimental study and modeling of bubble collisions

Rémi Revellin [1], Bruno Agostini [2], John R. Thome *

EPFL, STI, ISE, LTCM, ME G1 464, Station 9, CH-1015 Lausanne, Switzerland

Received 15 February 2007; received in revised form 17 July 2007

Abstract

The collision of elongated bubbles has been studied along adiabatic glass microchannels of 509 and 790 μm internal diameters for refrigerant R-134a. The slug flow regime obtained here comes from the nucleation process inside a micro-evaporator located upstream. Using an optical measurement technique based on two lasers and two photodiodes, it was possible to determine the vapor bubble length distributions at the exit of the micro-evaporator and 70 mm downstream and thus characterize both diabatic and adiabatic bubble collisions. The database includes 412 coupled sets of distributions involving thousands of bubbles. Half of the database has been obtained under diabatic conditions and the second half under adiabatic conditions.

A model for predicting the collision of elongated bubbles in microchannels (and their coalescence into longer bubbles) is proposed here and applied to the bubble length distribution at the exit of the micro-evaporator to determine the bubble length distribution along the glass microchannel. Presently, 81% of the entire database are predicted by the model with a tolerance of ±20% on the lengths of vapor bubbles. The test of Kolmogorov–Smirnov is used to compare the experimental and theoretical distributions. Assuming an initial mean bubble length, it was possible to simulate the sharp peak in bubble frequencies observed experimentally, capturing both the location and magnitude of these peaks.
© 2007 Elsevier Ltd. All rights reserved.

Keywords: Microchannels; Bubble collision; Two-phase flow; Velocity; Elongated bubble

1. Introduction

Elongated bubble flow (also named slug flow) is very often encountered in microchannels because it occurs over a wide range of flow parameters (Wambsganss et al. (1993)). The vapor bubbles are approximately the same diameter as the tube as shown in Fig. 1a and can grow only lengthwise. The nose of the bubble has a characteristic hemispherical-like cap and the vapor in the bubbles is separated from the tube wall by a thin film of liquid. The liquid flow is contained mostly in the liquid slugs which separate successive vapor bubbles. The length of the vapor bubbles can vary considerably. Bubbly/slug flow is also a vapor–liquid flow pattern which takes place inside microchannels when some vapor bubbles are smaller in length than the tube diameter as observed in Fig. 1b. Collision of bubbles in microchannels, which is a one-dimensional phenomena because of the channel's restriction on the flow, has been observed experimentally by Revellin et al. (2006) and appears to be one of the most important parameters influencing flow pattern transition (Revellin and Thome (2006)). Bubble collision occurs in microchannels when a longer bubble collides with a smaller bubble ahead of it due to its higher velocity, coalescing and forming one longer bubble. Agostini et al. (2007) in Part I of this study have experimentally demonstrated that bubble length has a direct influence on a bubble's velocity. The longer the vapor bubble, the faster it travels (up to a certain point where a plateau is reached). They also proposed a model to explain and predict bubble velocities.

* Corresponding author. Tel.: +41 21 693 5981; fax: +41 21 693 5960.
E-mail address: john.thome@epfl.ch (J.R. Thome).
[1] Co-Authors.
[2] Co-Authors.

0301-9322/$ - see front matter © 2007 Elsevier Ltd. All rights reserved.
doi:10.1016/j.ijmultiphaseflow.2007.07.006

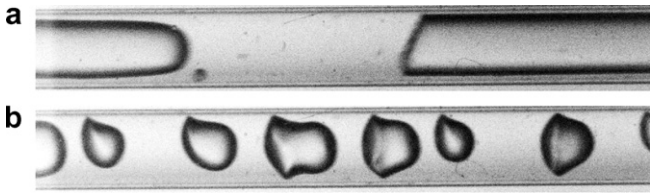

Fig. 1. Flow patterns for R-134a, $D = 509$ μm, $G = 500$ kg/m^2 s, $L_{MEV} = 70.7$ mm, $T_{sat} = 30$ °C and $\Delta T_{sub} = 3$ °C at entrance to heater: (a) slug flow at $x_{MEV,out} = 11\%$ (b) bubbly/slug flow at $x_{MEV,out} = 4\%$.

Bubble collision has been studied by many authors but most of the time for gas–liquid flows in vertical macrochannels and seldom in horizontal ones. For example, Majumder et al. (2006) and Gnotke et al. (2003) have investigated the collision of small bubbles in turbulent bubbly flow in a bubble column. In this case the size of the bubbles was much smaller than that of the tube. It was found by Majumder et al. (2006) that the bubble size distribution at any axial position along the tube was best fitted by a log-normal distribution and a correlation was proposed to predict bubble collision in such systems. Gnotke et al. (2003) highlighted the simultaneous occurrence of bubble collision and break-up phenomena and studied the influence of the level of turbulence in the liquid on these processes.

Talvy et al. (2000) observed the interaction between two consecutive elongated bubbles rising in a stagnant liquid in a 25 mm diameter vertical pipe. They experimentally found that the trailing bubble did not affect the motion of the leading one but that the trailing bubble, on the other hand, was sensitive to the velocity distortion created by the wake of the leading bubble. The acceleration of the trailing bubble was quite prominent in the near wake of the leading elongated bubble and was affected even at distances exceeding 50 pipe diameters in some cases. Furthermore, strong deformations and oscillations of the trailing bubble's nose were observed that were related to the quasi-resonant oscillations of the tail of the lead bubble.

Pinto et al. (1998) studied the collision of two gas slugs rising in a co-current flowing liquid in vertical tubes of 22, 32 and 52 mm internal diameter. It was found that the minimum distance between slugs above which there was no interaction is about 5D in the turbulent liquid flow regime. In the laminar flow regime two different behaviours were observed. If the ratio between the average velocity in the fully developed film around the bubble and the average velocity in the main liquid was greater than 25, collision between slugs was observed and the minimum distance between slugs above which there was no interaction is about 10D. If the value of that ratio is lower than 25 and the initial distance between slugs is greater than the wake length of the leading slug, the distance between bubbles increases during their rising in the column and bubble collision was not observed. The length of the wake was found to be about 5D whatever type of liquid flow regime.

Shemer et al. (2006) investigated the movement of two consecutive Taylor bubbles in 14 and 26 mm vertical pipes. They demonstrated that the unsteady velocity field in the liquid ahead of a trailing bubble affected both its propagation velocity and its shape. Their results support the hypothesis that the trailing bubble velocity is a superposition of the maximum velocity in the liquid and the bubble drift velocity due to buoyancy. However, it was measured that if the initial spacing between the bubbles was larger than about 7–10 pipe diameters, then the distance between the bubbles increases in the process of their propagation along the pipe.

Alternatively, some studies focus on the prediction of slug length distribution, which is an essential parameter to predict bubble collision. Barnea and Taitel (1993) proposed a model for slug distribution in gas–liquid slug flow in macrotubes that is able to calculate the slug length distribution at any desired distance along the pipe. The model assumes a random distribution at the inlet of the pipe and it calculates the increase or decrease in each individual slug length, including the disappearance of the short slugs, as they move downstream. The model is based on the bubble overtaking mechanism that occurs due to the fact that the translational velocity of an elongated bubble behind short slugs is considerably higher than that behind long slugs. It has also been shown that the evolution of the length distribution along the pipe is not sensitive to the slug length distribution at the pipe entrance. Finally, the slug length distribution in the developed region seems to follow approximately the log normal shape.

Cook and Behnia (2000) studied the statistical distribution of slug lengths in a gas–liquid flow in a near horizontal 50 mm diameter tube. Their data cover both stagnant and turbulent flowing liquid, in both the elongated bubble and slug flow regime. Their data shows that all the turbulent flow results may be correlated by the same expression regardless of the value of the slug liquid Reynolds number. In all cases, the minimum stable slug length was found to be close to 10 diameters in length.

To the best of our knowledge, Razzaque et al. (2003) published the only study about the bubble collision phenomenon during two-phase flow in horizontal pipes. Their experimental study was performed in a 25.4 mm tube to evaluate the development of the bubble size distribution in a horizontal turbulent flow of an air–water system. It was shown that the lognormal bubble size distribution was also valid for bubble collision dominant turbulent pipe flow, particularly at high water velocity. At lower water velocity, the distribution deviated slightly at both ends (large and small) from the lognormal shape.

As a conclusion, it is shown that many studies exist on the topics of vapor bubble length distribution and bubble collision, but all of them in macrochannels and for gas–liquid flow. Most of them focused on Taylor bubbles rising in a vertical channel. These different studies generally agree on the fact that the trailing bubble is affected by the wake of the leading bubble so that the length of the liquid slug between them is an important parameter controlling bubble collision. The minimal slug length above which the

trailing bubble is affected by the leading bubble varied from 5 to 10 diameters. Besides, the bubble length distribution was always found to follow a lognormal shape. On the other hand, the collision of elongated vapor bubbles in horizontal microchannels has not yet been studied. The main differences with the studies cited above is that there is no buoyancy effect and the confinement of the bubble creates a very thin liquid layer around the bubbles. Furthermore, in order to be as close as possible to conditions in a micro-evaporator, we chose to perform the present experiments with flow boiling of a refrigerant; thus the bubble length distribution is created by nucleation and bubble growth and is not dependent on the design of a gas–liquid mixing device. Moreover, the bubbles are created with refrigerant vapor and not a soluble gas. Experimental observations and modeling of collision of elongated bubbles in horizontal microchannels is the objective of this paper.

2. Description of the test facility

The microchannel test facility was described in Part I of this paper.

3. Optical measurement technique

An optical method to count bubbles and determine the two-phase flow characteristics has been used, which has previously been described in Revellin et al. (2006). The experimental setup consisted of two laser beams, with a power less than 1 mW, directed through the glass visualization tube and the fluid inside at two different locations, separated by a distance of $\Delta L_{\text{Laser}} = 70.63$ mm as presented in Fig. 2. Two lenses focused the laser beams to the middle of the microtube. Two photodiodes on the opposite side of the microtube, their faces painted over to leave only a vertical 1 mm wide opening in the middle to isolate the signal, measured the intensity of the light. They were connected to a *National Instruments* SCXI acquisition system using a scan rate of 10,000 measurements/s to measure the resulting voltage signals from the two diodes. A micropositioning system was used to align the laser beams with the lenses and photodiodes. The laser beams interact locally with the structure of the flow and by signal processing, it was possible to determine the velocity, length and frequency of vapor bubbles. The signals from the diodes obtained by this technique for the different flow regimes are similar to those obtained by Lowe and Rezkallah (1999) using a void fraction probe for a microgravity air/water two-phase flow in a 9.525 mm tube. Fig. 3 shows an example of the voltage signal for a slug flow regime. Low voltage corresponds to liquid and high voltage to liquid and vapor (an elongated bubble). The signal processing of our optical measurements consisted of several steps and are summarized in Revellin et al. (2006).

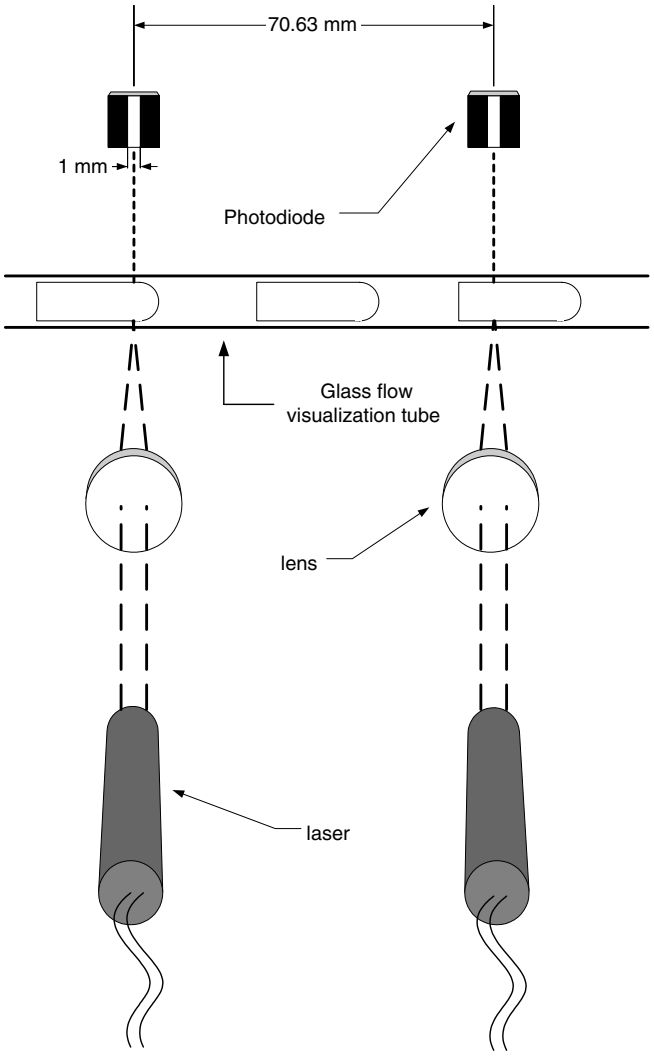

Fig. 2. Schematic diagram of the laser setup.

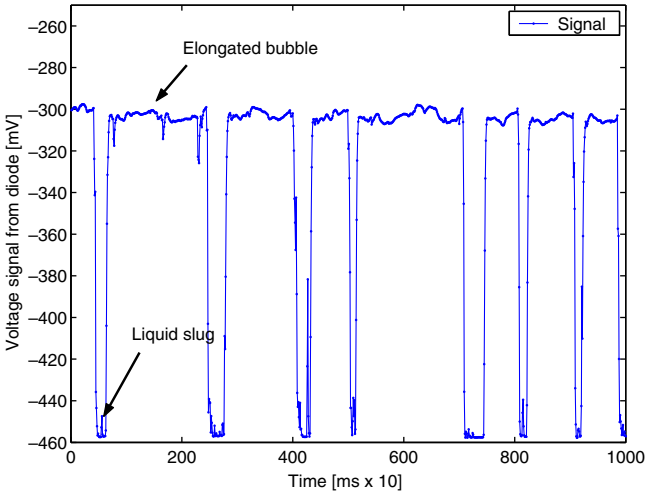

Fig. 3. Example of a voltage signal of the diode versus time for a elongated bubble flow regime.

4. Experimental results

With the optical measurement technique, it is possible to plot the distribution of elongated bubbles at laser 1 resulting from a diabatic two-phase flow exiting our micro-evaporator, and also the corresponding distribution obtained at laser 2 which are obtained under adiabatic conditions. Fig. 4a shows the experimental distribution of the vapor bubbles at laser 1 obtained under diabatic conditions. After a distance of approximately 70 mm downstream, the bubble collision effect can be observed in the distribution of vapor bubbles represented in Fig. 4b. Bubbles collide, and as a result, the number of vapor bubbles decreases and longer vapor bubbles appear. In this example, the bubble collision rate is 214 bubbles/s. All together, 412 sets of such distributions have been studied for lasers 1 and 2. The flow regimes studied here were bubbly/slug and slug flow regimes in 509 and 790 μm internal diameter tubes (bubbly flow was defined here as bubbles whose lengths were shorter than the channel diameter while slug flow was for bubbles longer than the diameter). The experimental conditions are summarized in Table 1. It is of importance to note here that half of the database has been obtained under diabatic conditions (laser 1) whereas the second half has been measured under adiabatic conditions (laser 2).

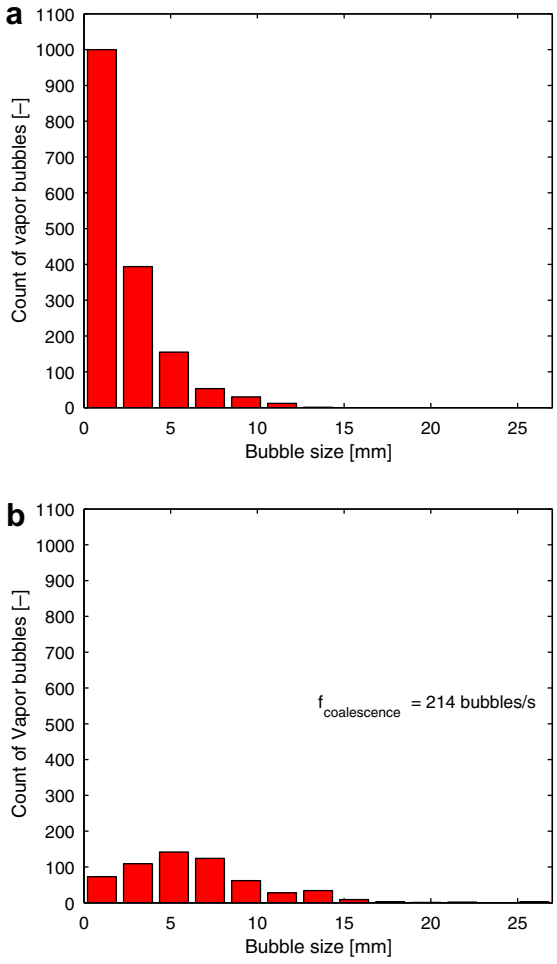

Fig. 4. Distribution of vapor bubbles for R-134a, $D = 790$ μm, $G = 500$ kg/m^2 s, $x = 7\%$, $L_{MEV} = 70.88$ mm, $\Delta T_{sub} = 3$ °C and $T_{sat} = 30$ °C: (a) Experimental distribution at laser 1. (b) Experimental distribution at laser 2 taken at the same time as laser 1.

Table 1
Experimental conditions and uncertainties (this Table refers to laser experiments whereas the Table of Part I refers to video experiments)

Parameter	Values	Uncertainties	Units
Fluid	R-134	–	–
D	509, 790	±1%	μm
$\frac{e}{D}$	<0.002%	–	–
L_{MEV}	30–70.88	<2.5%	mm
G	200–1500	±2%	kg/m^2 s
q	3.13–112.4	<5.7%	kW/m^2
T_{sat}	26–35	±0.1	°C
P_{sat}	6.9–8.9	<0.07%	bar
ΔT_{sub}	2–5	±0.1	°C
$x_{MEV,out}$	1–34	5.6%	–

5. Description of the model

As observed experimentally, collision of vapor bubbles is an important parameter that modifies the vapor bubble length distributions along a tube. There is a direct influence between the bubble length L_G and the bubble velocity U_G in microchannels. The following relation of Agostini et al. (2007) in Part I developed under diabatic conditions, shows the dependence between U_G and L_G:

$$U_G = \frac{D \cdot \gamma}{1 + \frac{C}{Co}} \frac{1 - \exp\left(\frac{-2 \cdot f_i \cdot L_G}{D}\right)}{2 \cdot f_i} + U_h \quad (1)$$

where C is a constant equal to -0.58, f_i is the interfacial friction factor expressed by the conventional relations (see Part I), U_h is the homogeneous velocity and Co is the confinement number given by Eq. (2):

$$Co = \left(\frac{g(\rho_L - \rho_G)D^2}{\sigma}\right)^{-1/2} \quad (2)$$

with σ the surface tension, g the acceleration of gravity and ρ_L and ρ_G respectively the liquid and vapor densities.

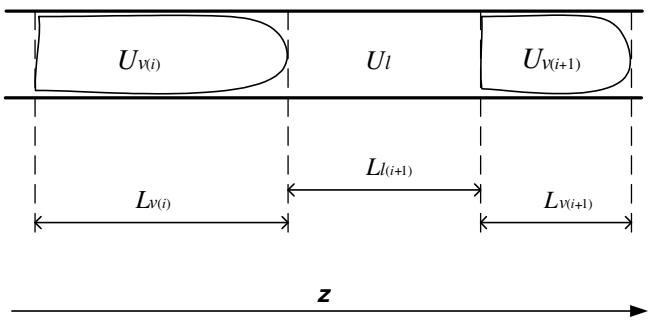

Fig. 5. Schematic of vapor bubbles and liquid slug.

γ is defined by Eq. (3):

$$\gamma = \frac{4q}{D \cdot h_{LG} \cdot \rho_G} \tag{3}$$

with q the heat flux and h_{LG} the latent heat of vaporization.

The main step of the present model is to determine a criterion for collision of two sequential bubbles of different lengths. We assume that the collision between two vapor bubbles occurs if the trailing vapor bubble travels faster than the vapor bubble ahead of it in a microchannel.

Thus, now consider a vapor bubble with a velocity $U_{G_{i+1}}$ preceded by a liquid slug of length $L_{L_{i+1}}$ and a vapor bubble of velocity U_{G_i} as shown in Fig. 5. The time that the vapor bubble $i+1$ needs to travel from points 1 to 2 downstream separated by a distance Δz is

$$t_{G_{i+1}} = \frac{\Delta z}{U_{G_{i+1}}} \tag{4}$$

There is collision if the vapor bubble i travels faster than the vapor bubble $i+1$ according to the following criterion:

$$t_{G_{i+1}} U_{G_i} - t_{G_{i+1}} U_{G_{i+1}} \geqslant L_{L_{i+1}} \tag{5}$$

or

$$L_{L_{i+1}} - \frac{\Delta z}{U_{G_{i+1}}}(U_{G_i} - U_{G_{i+1}}) \leqslant 0 \tag{6}$$

This criterion applied to a known distribution of vapor bubbles and liquid slugs at the inlet of a microchannel can be used to predict the distribution of the flow at the outlet of the microchannel in terms of length, velocity and frequency of bubbles. The length of the tube is discretized in order to take numerically into account the multiple collision of the bubbles. This model can be applied to the distribution of vapor bubbles at laser 1 to obtain a theoretical distribution at laser 2 and compare that with the experimental distribution at laser 2.

Fig. 6 shows the bubble collision model applied to the results depicted in Part 4 (Fig. 4a and b). It is observed that the theoretical and experimental distributions at laser 2 are quite close to each other. The maximum of the distribution is about 200 bubbles for both cases (instead of 1000 in the original distribution at laser 1), long vapor bubbles appeared (lengths from 15 to 30 mm) and short ones disappeared (lengths from 0 to 5 mm). The number of bubbles around the 5 mm length, falls to about $1 \setminus 10$ as many and this is predicted by the model. The theoretical collision rate is 181 bubbles/s compared to the experimental rate of 214.

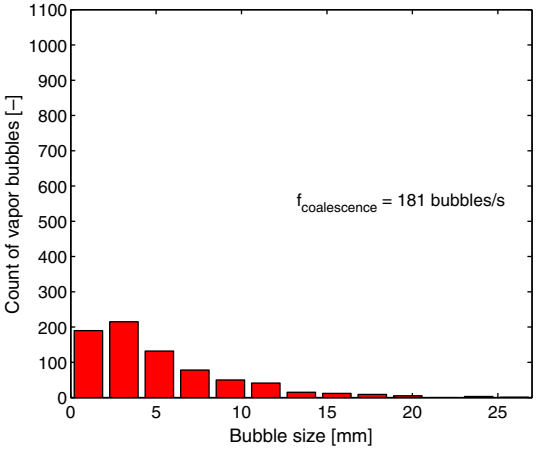

Fig. 6. Theoretical distribution of vapor bubbles at laser 2 for R-134a, $D = 790$ μm, $G = 500$ kg/m^2 s, $x = 7\%$, $L_{MEV} = 70.88$ mm, $\Delta T_{sub} = 3$ °C and $T_{sat} = 30$ °C.

6. Definition of an objective method to compare experimental and theoretical bubble length distributions

In order to assess the performances of this model, an objective criterion is needed. Several methods can be used to compare two distributions. For example, Cook and Behnia (2000) compared their experimental and predicted bubble length distributions with the mean and variance only, which is not a vigorous goodness-of-fit test since two distributions can have the same mean and variance with completely different shapes. The minimum test should be a comparison of mean, variance, kurtosis and skewness. However, even with those 4 parameters, an objective acceptance or rejection criterion is still needed.

Another widely used method is the χ_2 test. However the χ_2 test is primarily intended for comparing discretized distributions, which is not the case here since the model is a continuous function. The χ_2 test is generally considered to be a *weak* test. Firstly, the theoretical distribution has to be discretized in a number of classes comprised between 10 and 20 with not less than 5 elements in any class. If a class has less than 5 elements, it has to be regrouped with another adjacent class. Thus the discretization can generally be tweaked to give acceptable results. Secondly, the χ_2 test averages the difference between the experimental and theoretical distributions over the number of classes so that large local differences will be leveled and deemed acceptable by the test. For these reasons, the χ_2 test is considered not appropriate for the present study.

The best objective test applicable here for goodness-of-fit tests when one deals with a continuous distribution and does not require adjustment of any parameters of the model with the tested experimental data is the Kolmogorov–Smirnov test. Suppose that we have a sample of bubble lengths $L_1, \ldots, L_n$ with a distribution $\mathscr{P}_n$ and we would like to test the hypothesis that $\mathscr{P}_n$ is equal to a theoretical distribution $\mathscr{P}$. Let us denote

$$F(x) = \mathscr{P}(L \leqslant x) \tag{7}$$

as the cumulative distribution function predicted by the model and consider the experimental cumulative distribution function to be

$$F_n(x) = \mathscr{P}_n(L \leqslant x) = \frac{1}{n}\sum_{i=1}^{n} I(L_i \leqslant x) \tag{8}$$

where I is the function that counts the number of bubbles having lengths less than x. $F_n(x)$ is simply the proportion

of the bubble lengths below level x. Then the Kolmogorov–Smirnov statistic is defined by:

$$D_n \equiv \sqrt{n} \cdot \sup_{0<x<+\infty} |F_n(x) - F(x)| \quad (9)$$

The Kolmogorov–Smirnov test rejects the theoretical distribution if D_n is too large. The test itself answers to the question: what is the probability of being wrong if I reject the theoretical distribution? The rejection threshold depends on the level of significance α. Generally α is taken equal to 5%, which means that if the theoretical distribution is rejected, the probability that it should have been accepted is 5%. The values of the Kolmogorov–Smirnov statistic $D(n,\alpha)$ are tabulated (it is a function of the size of the sample n and of the level of significance α). Finally the test is: the theoretical distribution is rejected if $D_n > D(n,\alpha)$ and accepted if $D_n < D(n,\alpha)$. This is illustrated in Fig. 7: a comparison of experimental and theoretical cumulative distributions is shown when the Kolmogorov–Smirnov test accepts the theoretical distribution (a) and when it is rejected (b). Example (a) is related to the distributions showed previously.

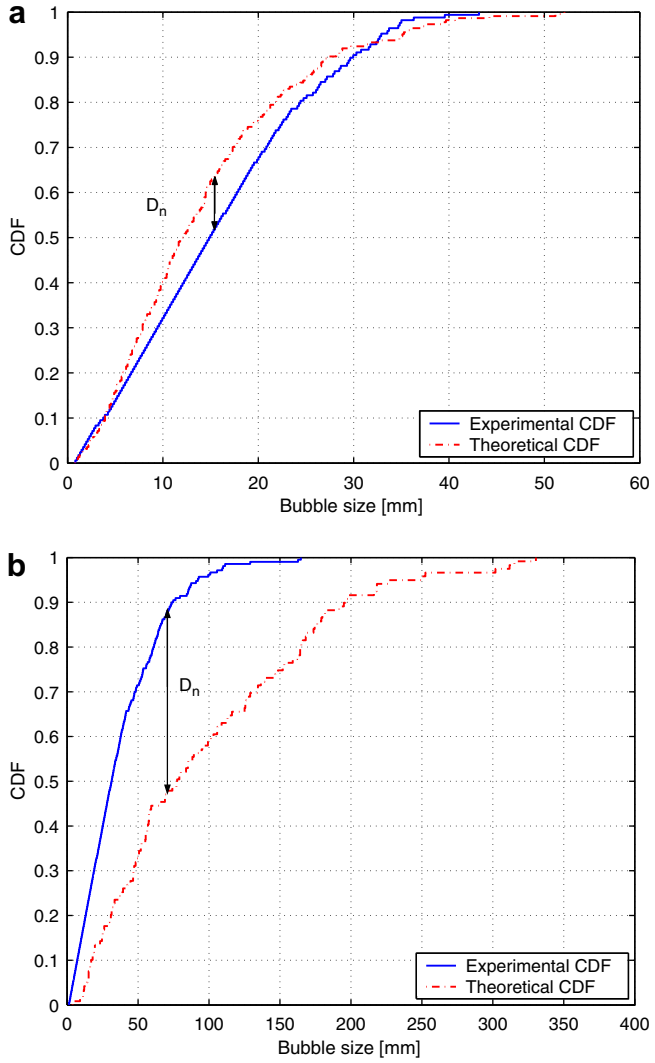

Fig. 7. Comparison of experimental and theoretical cumulative distribution functions (R-134a, $D = 790$ μm, $T_{sat} = 30$ °C, $L_{MEV} = 70.88$ mm): (a) D_n is small so the Kolmogorov–Smirnov test accepts the distribution ($G = 500$ kg/m^2 s, $x = 7\%$), (b) D_n is too large so the Kolmogorov–Smirnov test rejects the distribution ($G = 1200$ kg/m^2 s, $x = 7\%$).

The Kolmogorov–Smirnov test provides an easy and objective test to compare an experimental and a theoretical continuous distribution. No hypothesis is made and this test is accepted as a *strong* test by the mathematical community so that we recommend it as a standard tool for bubble length distributions.

7. Comparison with experimental data

In order to validate the model with the 412 experimental distributions, a tolerance of ±20% on the vapor bubble lengths has been applied. This tolerance corresponds to the uncertainty on the length of the shortest bubbles. The coupling of the distributions (experimental and theoretical ones) has then been submitted to the test of Kolmogorov–Smirnov. It was found that 81% of the entire database was predicted by the model with a tolerance of ±20% on the lengths of vapor bubbles. The model is thus validated for the bubbly/slug and slug flow regimes.

Fig. 8 shows the experimental length distribution of vapor bubbles at laser 1 and 2 as well as the theoretical distribution of vapor bubbles at laser 2 for the 509 μm diameter tube. The model predicts the experimental distribution at laser 2 with a tolerance of ±20% on the lengths of vapor bubbles according to the test of Kolmogorov–Smirnov. The frequency of bubble collision is measured to be 22 and predicted to be 21 bubbles/s. It is interesting to see that the small vapor bubbles disappear due to their collision and the creation of longer bubbles. For example, the model predicts the appearance of a 50 mm long bubble that appears also in the experimental distribution. Notably, the model also predicts the disappearance of almost all the 0–5 mm long bubbles, which also happens in the experimental distribution.

Another example of distributions is given by Fig. 9 for vapor bubbles flowing in the 509 μm diameter tube with a mass flux of 1000 kg/m^2 s. The appearance of vapor bubbles, whose lengths are greater than 20 mm, can be observed experimentally and theoretically. Furthermore, the decrease of the number of small vapor bubbles with lengths less than 5 mm is also observable. The frequency of bubble collision is around 65 bubbles/s in both cases.

Fig. 10 shows an example of distributions of vapor bubbles flowing in the 790 μm diameter tube with a mass flux of 200 kg/m^2 s. Here again, the model predicts the data with a tolerance of ±20% on the lengths of vapor bubbles according to the test of Kolmogorov–Smirnov. The predicted frequency of bubble collision is 60.7 bubbles/s, close to the 50.5 bubbles/s measured experimentally. The appearance of bubbles having lengths of around 85 mm is predicted by the model and confirmed experimentally.

Fig. 11 shows the variation of the bubble frequencies as a function of the vapor quality. As explained by Revellin

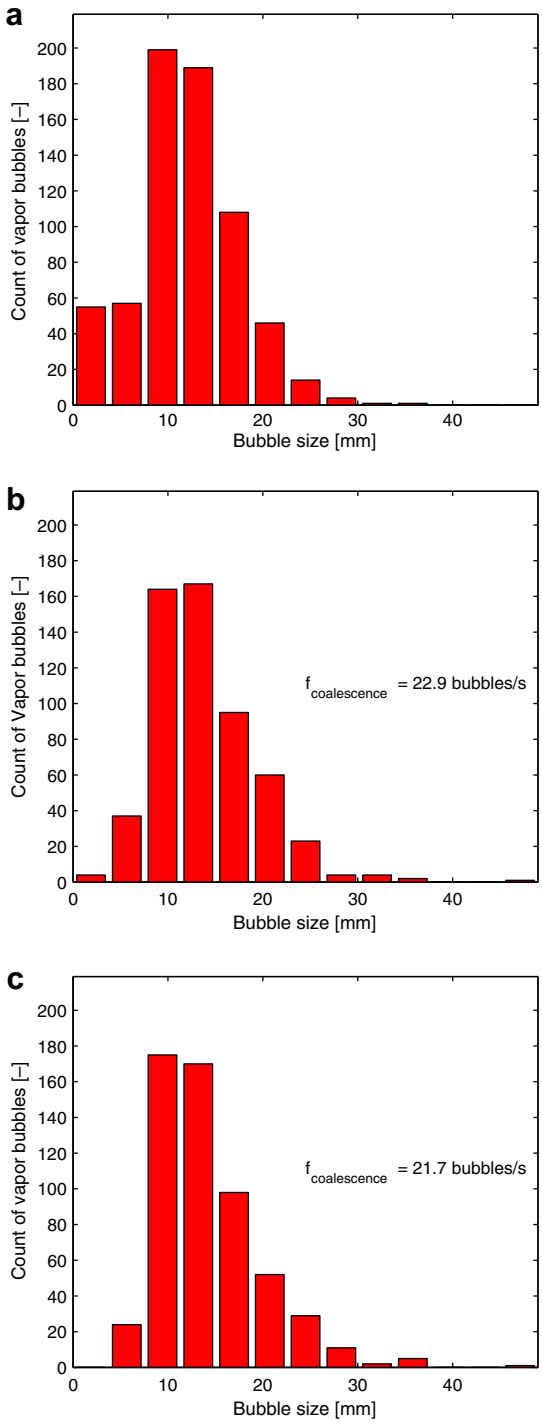

Fig. 8. Distribution of vapor bubbles for R-134a, $D = 509$ μm, $G = 500$ kg/m^2 s, $x = 11\%$, $L_{MEV} = 70.7$ mm, $\Delta T_{sub} = 3$ °C and $T_{sat} = 30$ °C: (a) Experimental distribution at laser 1. (b) Experimental distribution at laser 2. (c) Theoretical distribution at laser 2.

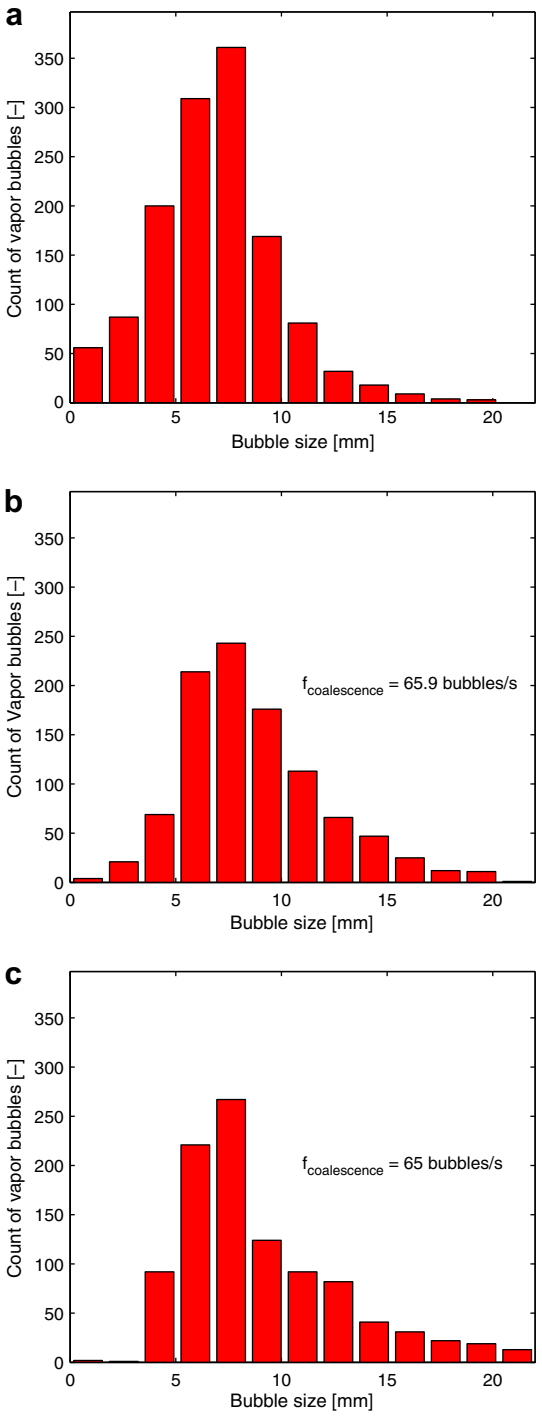

Fig. 9. Distribution of vapor bubbles for R-134a, $D = 509$ μm, $G = 1000$ kg/m^2 s, $x = 5\%$, $L_{MEV} = 70.7$ mm, $\Delta T_{sub} = 3$ °C and $T_{sat} = 30$ °C: (a) Experimental distribution at laser 1. (b) Experimental distribution at laser 2. (c) Theoretical distribution at laser 2.

and Thome (2006), the frequency increases rapidly with vapor quality (or heat flux in the evaporator), reaches a maximum and then decreases sharply. The upward slope corresponds to the predominance of bubble generation due to the boiling process over the hydrodynamic process of bubble collision. The downward slope is related to the predominance of the bubble collision phenomena over that of bubble generation. Fig. 11 shows the bubble frequencies for bubbles passing through lasers 1 and 2 as well as the bubble frequencies at laser 2 calculated from the model with the frequency curve at laser 1 as input. It is clear that the model is able to correctly predict the experimental data for the frequencies at laser 2. It is also interesting to see the

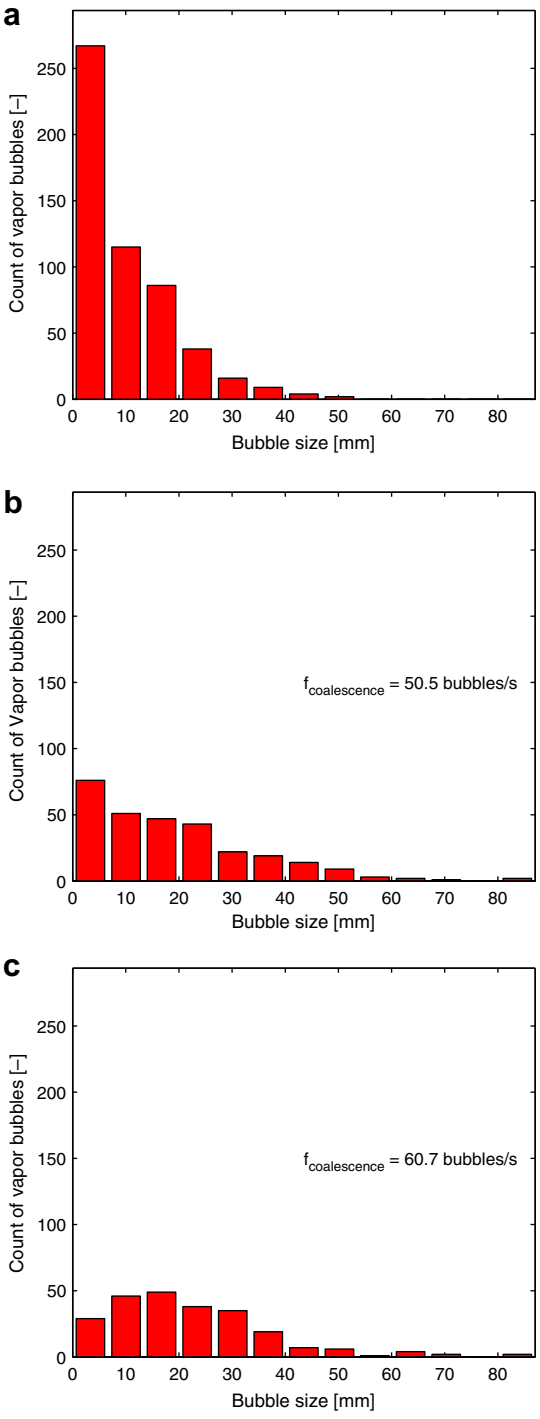

Fig. 10. Distribution of vapor bubbles for R-134a, $D = 790$ μm, $G = 200$ kg/m^2 s, $x = 18\%$, $L_{MEV} = 70.88$ mm, $\Delta T_{sub} = 3$ °C and $T_{sat} = 30$ °C: (a) Experimental distribution at laser 1; (b) Experimental distribution at laser 2 and (c) Theoretical distribution at laser 2.

adiabatic collision effect between lasers 1 and 2 characterized by a lower frequency at laser 2.

8. Modeling of diabatic bubble collision

As explained earlier, half of the database (from laser 1) has been obtained under diabatic conditions. By consequence, after modeling the adiabatic bubble collision, it seems interesting to model the bubble collision phenomena under diabatic conditions and compare with the 412 distributions measured at laser 1. Fig. 11 shows that the outlet bubble frequency curve as a function of the outlet vapor quality at laser 1 has a bell shape with a sharp peak. The application of the preceding adiabatic model allows one to predict the evolution of this curve along an adiabatic tube, but does not predict the existence of the peak itself. That would mean that using Eq. (1) for predicting the difference in bubble velocities is not sufficient to explain bubble collision in a diabatic flow. In order to predict this peak, a diabatic bubble collision model is needed, including bubble growth effects due to vaporization. This model can be applied along the evaporator, with an artificial bubble length distribution as input to predict the bubble frequencies leaving the micro-evaporator at laser 1. A simplified model is presented that ignores the small fraction of liquid in the liquid layer between the elongated bubbles and the tube wall. The different contributions to diabatic bubble collision during a time step of Δt are presented in Fig. 12:

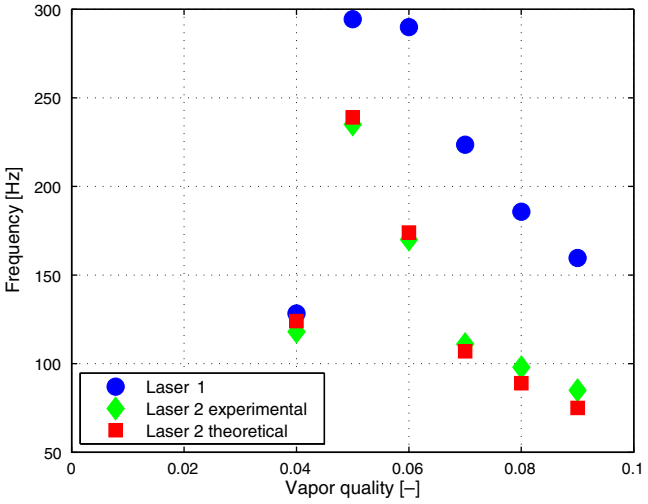

Fig. 11. Measured and predicted bubble frequencies as a function of vapor quality for R-134a, $D = 790$ μm, $G = 350$ kg/m^2 s, $L_{MEV} = 70.88$ mm, $\Delta T_{sub} = 3$ °C and $T_{sat} = 30$ °C.

(1) at time t, two successive elongated bubbles of respective lengths $L_G^i(t)$ and $L_G^{i+1}(t)$ are separated by a liquid slug of length $L_L^i(t)$,
(2) during Δt some liquid is evaporated thus producing an increase in length ΔL_G^i of each bubble while the liquid slug length decreases by $\Delta L_{L,x}^i$,
(3) the elongated bubble length increase ΔL_G^i causes a corresponding displacement of liquid $\Delta L_{L,G}^i$ because of the new volume occupied by the bubble,
(4) meanwhile, as during the adiabatic collision, the bubbles travel with different speeds $U_G^i(t)$ depending on their length. The distance traveled by a bubble during Δt causes a displacement of liquid $\Delta L_{L,U}^i$ around the bubble.

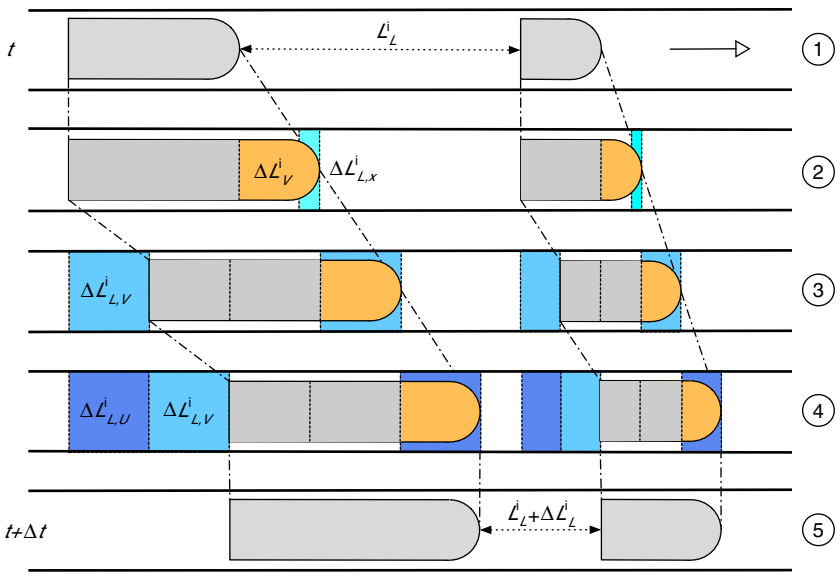

Fig. 12. Successive steps of the diabatic bubble collision process taken into account by the model: (1) initial bubble distribution at time t, (2) liquid vaporization, (3) bubble volume expansion, (4) bubble velocity differences and (5) final bubble distribution at time $t+\Delta t$.

(5) finally, because of these three contributions, the length of the liquid slug separating the two bubbles at $t+\Delta t$ is $L^i_{\mathrm{L}}(t+\Delta t) = L^i_{\mathrm{L}}(t) - \Delta L^i_{\mathrm{L}}$.

Only the contribution (4) is the cause of bubble collision under adiabatic conditions. The adiabatic bubble collision model is thus a special case of the diabatic bubble collision model, the latter being more general. The different contributions for bubble number i can be calculated as follows, where q is a uniform heat flux from the channel wall into the fluid:

$$\begin{aligned}
\Delta L^i_{\mathrm{G}} &= \left(L^i_{\mathrm{G}}(t) + L^i_{\mathrm{L}}(t)\right)\cdot\frac{4q}{h_{\mathrm{LG}}\cdot D\cdot\rho_{\mathrm{G}}}\cdot\Delta t\\
\Delta L^i_{\mathrm{L},x} &= -\left(L^i_{\mathrm{G}}(t) + L^i_{\mathrm{L}}(t)\right)\cdot\frac{4q}{h_{\mathrm{LG}}\cdot D\cdot\rho_{\mathrm{L}}}\cdot\Delta t\\
\Delta L^i_{\mathrm{L,G}} &= -\Delta L^i_{\mathrm{G}}\\
\Delta L^i_{\mathrm{L,U}} &= -U^i_{\mathrm{G}}(t)\cdot\Delta t
\end{aligned} \tag{10}$$

Finally, the length variation of the liquid slug number i (situated between bubble number i and bubble number $i+1$) during Δt is:

$$\Delta L^i_{\mathrm{L}} = \Delta L^i_{L,x} - \left(\Delta L^{i+1}_{\mathrm{L,G}} - \Delta L^i_{\mathrm{L,G}}\right) - \left(\Delta L^{i+1}_{\mathrm{L,U}} - \Delta L^i_{\mathrm{L,U}}\right) \tag{11}$$

so that the liquid slug number i length at $t+\Delta t$ is

$$\begin{aligned}
L^i_{\mathrm{L}}(t+\Delta t) &= L^i_{\mathrm{L}}(t+\Delta t) + \Delta L^i_{\mathrm{L}}\\
&= L^i_{\mathrm{L}}(t) - \left(L^i_{\mathrm{G}}(t) + L^i_{\mathrm{L}}(t)\right)\cdot\frac{4q}{h_{\mathrm{LG}}\cdot D\cdot\rho_{\mathrm{L}}}\cdot\Delta t\\
&\quad - \left(\Delta L^{i+1}_{\mathrm{G}} - \Delta L^i_{\mathrm{G}}\right) - \left(U^{i+1}_{\mathrm{G}}(t) - U^i_{\mathrm{G}}(t)\right)\cdot\Delta t
\end{aligned} \tag{12}$$

and the elongated bubble number i length at $t+\Delta t$ is

$$L^i_{\mathrm{G}}(t+\Delta t) = L^i_{\mathrm{G}}(t) + \left(L^i_{\mathrm{G}}(t) + L^i_{\mathrm{L}}(t)\right)\cdot\frac{4q}{h_{\mathrm{LG}}\cdot D\cdot\rho_{\mathrm{G}}}\cdot\Delta t \tag{13}$$

To implement this model it is necessary to start with a known bubble length distribution DL_{G} and liquid slug length distribution DL_{L}, and apply the model along a tube length L_{ev} where a uniform heat flux q is applied. Several authors like Majumder et al. (2006) showed that the bubble length distribution before the start of bubble collision was well predicted by a lognormal distribution. Thus, let us imagine that before the evaporator of length L_{ev} there is a pre-evaporator whose length is 10% of L_{ev}, which produces a lognormal bubble length distribution DL_{G} before any bubble collision can happen. The outlet bubble frequency curve usually stretches from 0% to 30% vapor quality so that the vapor quality at the outlet of this pre-evaporator would range from 0% to 3%. Since no bubble collision was observed on numerous high speed videos at such low vapor qualities, this assumption is reasonable.

In order to generate a lognormal distribution, we need to specify the average length $\overline{L}$ and the variance V. Since the vapor quality at the inlet of the evaporator (i.e. outlet of the pre-evaporator) x_{in} is specified, there is a relationship between the average and variance of the bubble length and liquid slug length distributions given by:

$$\begin{aligned}
\overline{L_{\mathrm{L}}} &= \frac{\rho_{\mathrm{G}}}{\rho_{\mathrm{L}}}\cdot\frac{1-x_{in}}{x_{\mathrm{in}}}\cdot\overline{L_{\mathrm{G}}}\\
V_{\mathrm{L}} &= \frac{\rho_{\mathrm{G}}}{\rho_{\mathrm{L}}}\cdot\frac{1-x_{\mathrm{in}}}{x_{\mathrm{in}}}\cdot V_{\mathrm{G}}.
\end{aligned} \tag{14}$$

Once these distributions are generated, each liquid slug of the distribution DL_{L} is inserted between two successive bubbles of the distribution DL_{G}, thus generating an artificial bubbly flow corresponding to a vapor quality of x_{in}.

The average bubble length and the variance are both fixed equal to 0.2D. These values were chosen so that the experimental maximal bubble frequency matches that predicted by the model. Although only a specific experimental setup would be able to provide these values, the chosen values seem reasonable for a bubbly flow. The heat flux is calculated to have the specified vapor quality x_{out} at the evaporator exit with:

$$q = \frac{G \cdot D \cdot h_{LG}}{4L_{ev}} \cdot x_{out}. \quad (15)$$

Distributions of 10,000 bubbles are generated, the evaporator length is discretized into 1000 elementary parts dz, the velocity of each bubble is calculated with Eq. (1) and the new bubble and liquid slug lengths at each time step $dt = dz \cdot U_h$ are calculated with Eqs. (12) and (13). Each time a liquid slug length L_L^i is equal to 0, bubble collision occurs and the two bubbles preceding and following the liquid slug are merged. For each outlet vapor quality, this process is repeated at every time step and for the 10,000 bubbles until every bubble has traveled the evaporator length. Finally the outlet bubble frequency can be calculated and plotted as a function of the evaporator outlet vapor quality. This model was implemented on a computer using Python 2.5 software.

Fig. 13 shows typical lognormal distributions of bubble and liquid slug lengths generated at the inlet of the evaporator and the corresponding distributions predicted by the model at the outlet, for $x_{out} = 0.1$, $D = 509$ μm, $G = 500$ kg/m^2 s, $T_{sat} = 3$ °C and $L_{ev} = 70.70$ mm (actually the subcooled length was subtracted in the calculations). It can be seen that at the outlet of the evaporator, both the

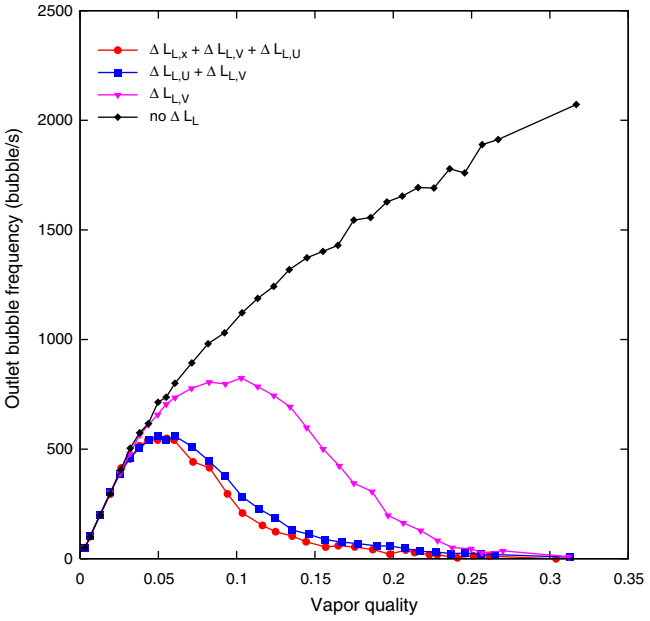

Fig. 14. Influence of the three contributions of evaporation in the diabatic bubble collision model on the outlet bubble frequency. The conditions are $D = 509$ μm, $G = 500$ kg/m^2 s, $T_{sat} = 30$ °C, $L_{ev} = 70.70$ mm.

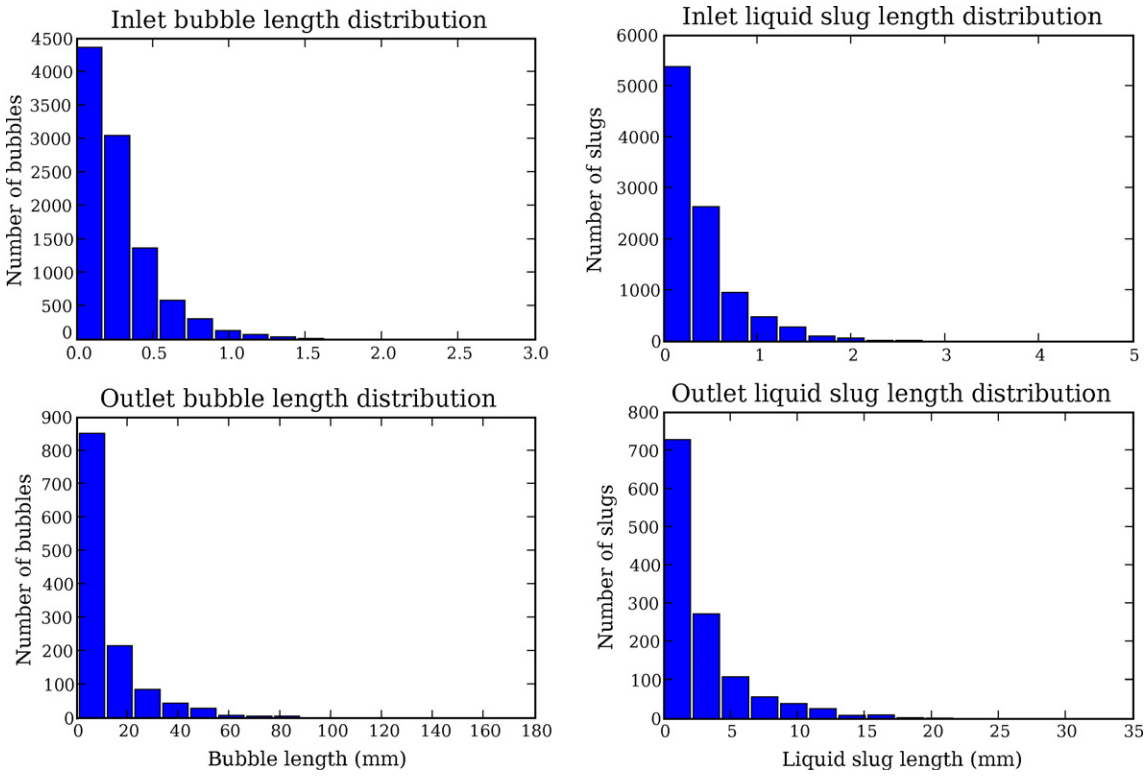

Fig. 13. Typical lognormal distributions generated for bubble (left) and liquid slug (right) lengths at the inlet of the evaporator (top) and distributions predicted by the model at the outlet (bottom). The conditions are $x_{out} = 0.1$, $D = 509$ μm, $G = 500$ kg/m^2 s, $T_{sat} = 30$ °C, $L_{ev} = 70.70$ mm.

number of bubbles and liquid slugs have decreased while their lengths have increased, which is the expected behavior. The influence of the three collision contributions (2), (3) and (4) on the bubble frequency at the outlet of the evaporator is shown in Fig. 14, for the same conditions but at various vapor qualities. The major contribution to diabatic bubble collision is the increase of the bubbles' volumes due to vaporization, since it yields the typical bell curve of the bubble frequency instead of a monotonically increasing curve that would be obtained if no bubble collision at all occurred. Then comes the bubble velocity difference contribution, which causes the bubble frequency to decrease faster with vapor quality. Finally, the disappearance of the vaporized liquid is nearly negligible, which is expected since the ratio of liquid to vapor density is about 35.

Fig. 15 shows a comparison between the bubble frequency versus vapor quality curve predicted by the diabatic bubble collision model and that measured under diabatic conditions at laser 1 by Revellin et al. (2006) for $D = 509$ μm, $G = 500$ kg/m^2 s, $T_{sat} = 30$ °C and $L_{ev} = 70.70$ mm. The general shape of the curve is well predicted with (i) the steep rise in frequency for $x < 0.05$, (ii) the peak followed by a steep decline for $0.05 < x < 0.13$, (iii) a slower frequency rate of decline for $x > 0.13$ and finally (iv) a frequency close to zero for $x > 0.25$ corresponding to the transition towards the annular flow pattern. The only notable difference is in region (ii) where the frequency decrease for $x > 0.05$ is steeper that expected compared to the prediction and the beginning of region (iii) which starts at a lower vapor quality for the experimental curve. However, given that this model relies on an hypothetical bubble length distribution, the agreement is good and proves that bubble collision is the controlling phenomenon during elongated bubble flow in microchannels and should therefore be taken into account for future flow pattern transition and heat transfer models. This peak actually represents one of the flow pattern transitions described in the recent diabatic flow pattern map proposed by Revellin et al. (2006) for microchannels.

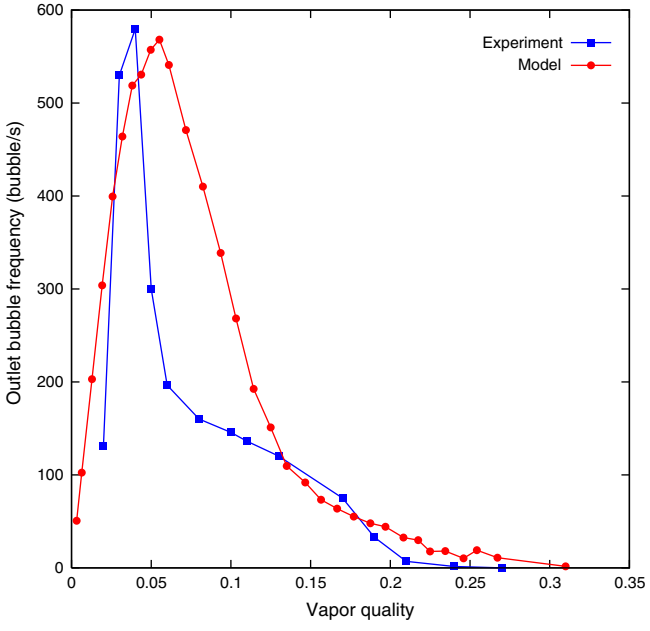

Fig. 15. Comparison between the bubble frequency versus vapor quality curve predicted by the diabatic bubble collision model and that measured by Revellin et al. (2006). The conditions are $D = 509$ μm, $G = 500$ kg/m^2 s, $T_{sat} = 30$ °C, $L_{ev} = 70.70$ mm.

9. Conclusion

The collision of elongated bubbles has been studied along adiabatic glass microchannels of 509 and 790 μm internal diameters for refrigerant R-134a. The slug flow regime obtained here comes from the nucleation process inside a micro-evaporator located upstream. Using an optical measurement technique based on two lasers and two photodiodes, it was possible to determine the vapor bubble length distributions at the exit of the micro-evaporator where the first laser is located on the glass tube and 70 mm downstream where the second laser is located. As a result, half of the database has been obtained under diabatic conditions whereas the second half has been collected under adiabatic conditions. Bubble collision occurs when a long bubble touches a shorter bubble ahead of it and forms only one longer bubble. The difference in velocities between the long and the short bubbles explains this phenomena. The longer the vapor bubble, the faster it travels. The database includes 412 couples of distributions at the laser locations.

A model for predicting collision of elongated bubbles in microchannels has been developed and applied to the bubble length distribution at the exit of the micro-evaporator to determine the bubble length distribution along the glass microchannel. It consists first of all of applying the model of Agostini et al. (2007) in Part I, which describes the relationship between the length and the velocity of elongated bubbles flowing in microchannels. Then a criterion for bubble collision is determined. As a result, it is possible to predict the vapor bubble length distribution 70 mm after the micro-evaporator downstream from the initial vapor bubble length distribution upstream at the exit of the micro-evaporator. Presently, 81% of the entire database are predicted by the model with a tolerance of ±20% on the lengths of vapor bubbles. The test of Kolmogorov–Smirnov is used to compare the experimental and theoretical distributions. This test is also recommended for any comparison of distributions in the future. Furthermore, modeling of diabatic bubble collision showed that it was able to predict the shape of the bubble frequency versus vapor quality curve, notably the frequency peak at low vapor quality. Extending the calculation out to higher vapor qualities it may also be possible to predict the location of complete bubble collision, i.e. the start of annular flow. Thus, the present model in Parts I and II are two crucial initial steps towards the development of a theoretically based diabatic flow pattern map for microchannels.

Acknowledgements

B. Agostini is supported by the Swiss Confederation under the CTI-project No. 6862.2 DCS-NM.

R. Revellin is supported by the Swiss National Science Foundation (SFN) grant number 20 111626/1.

References

Agostini, B., Revellin, R., Thome, J.R., 2007. Elongated bubbles in microchannels. Part i: Experimental study and modelization of elongated bubble velocity. Int. J. Multiphase Flow, In Review.

Barnea, D., Taitel, Y., 1993. A model for slug length distribution in gas–liquid flow. Int. J. Multiphase Flow 19, 829–838.

Cook, M., Behnia, M., 2000. Slug length prediction in near horizontal gas–liquid intermittent flow. Chem. Eng. Sci. 55, 2009–2018.

Gnotke, O., Benk, H., Loth, R., 2003. Experimental study on the number density distribution function in turbulent bubbly flows with coalescence and break-up. Exp. Therm. Fluid Sci. 27, 803–816.

Lowe, D.C., Rezkallah, K.S., 1999. Flow regime identification in microgravity two-phase flows using void fraction signals. Int. J. Multiphase Flow 25, 433–457.

Majumder, S., Kundu, G., Mukherjee, D., 2006. Bubble size distribution and gas—liquid interfacial area in a modified downflow bubble column. Chem. Eng. J. 122, 1–10.

Pinto, A.M.F.R., Pinheiro, M.N.C., Campos, J.B.L.M., 1998. Coalescence of two gas slugs rising in a co-current flowing liquid in vertical tubes. Chem. Eng. Sci. 53, 2973–2983.

Razzaque, M., Afacan, A., Liu, S., Nandakumar, K., Masliyah, J., Sanders, R., 2003. Bubble size in coalescence dominant regime of turbulent air–water flow through horizontal pipes. Int. J. Multiphase Flow 29, 1451–1471.

Revellin, R., Thome, J., 2006. New diabatic flow pattern map for evaporating flow in microchannels. In: 13th International Heat Transfer Conference. Sydney, Australia.

Revellin, R., Dupont, V., Ursenbacher, T., Thome, J.R., Zun, I., 2006. Characterization of diabatic two-phase flows in microchannels: low parameter results for R-134a in a 0.5 mm channel. Int. J. Multiphase Flow 32, 755–774.

Shemer, L., Gulitski, A., Barnea, D., 2006. Movement of two consecutive taylor bubbles in vertical pipes. In: 4th Japanese–European Two-Phase Flow Group Meeting. 24–28 September, Kyoto, Japan.

Talvy, C.A., Schemer, L., Barnea, D., 2000. On the interaction between two consecutive elongated bubbles in a vertical pipe. Int. J. Multiphase Flow 26, 1905–1923.

Wambsganss, M.W., France, D.M., Jendrzejczyk, J.A., Tran, T.N., 1993. Boiling heat transfer in a horizontal small-diameter tube. J. Heat Transfer 115, 963–972.